Emerald Rapid Prototyping Journal

Edge quality in Fused Deposition Modeling: II. Experimental verification

Journal:	*Rapid Prototyping Journal*
Manuscript ID	RPJ-02-2016-0021.R1
Manuscript Type:	Original Article
Keywords:	Fused deposition modelling, accuracy

Edge quality in Fused Deposition Modeling: II. Experimental verification

Abstract

Purpose – To provide an experimental evaluation of geometric errors on the edges of parts manufactured by the FDM process.
Design/methodology/approach – An experimental plan was conducted by building parts in ABS thermoplastic resin on a commercially available machine with given combinations of the three geometric variables (inclination, included and incidence angle) defined in the first part of the paper. Edges on built parts were inspected on a 2D non-contact profilometer to measure position and form errors.
Findings – The analysis of measurement results revealed that the edge-related variables have significant influences on the geometric errors. The interpretation of error variations with respect to the different angles confirmed the actual occurrence of the previously discussed error causes. As an additional result, quantitative predictions of the errors were provided as a function of angle values.
Research limitations/implications – The experimental results refer to fixed process settings (material, FDM machine, layer thickness, build parameters, scan strategies).
Originality/value – The two-part paper is apparently the first to have studied the edges of additively manufactured parts with respect to geometric accuracy, a widely studied topic for surface features.

Keywords

Additive manufacturing; fused deposition modeling; edge quality; geometric accuracy; defect prediction.

1 Introduction

Parts produced by additive manufacturing (AM) techniques often include edges with complex and variable profiles, whose geometric accuracy may raise some concern due to the limited detail resolution of the build processes. This is especially true for the Fused Deposition Modeling (FDM) process, where the thermoplastic material undergoes shrinkage upon solidification and cooling over a wide temperature interval, and the layer thickness is kept at relatively high values for productivity and cost reasons.
In order to satisfy design specifications related to functional or aesthetic requirements, engineers in charge of process planning should be able to predict the geometric errors on the edges of a FDM part. These may depend on many influence factors including the local geometry of the edge, the orientation of the part during the build process, and other parameters related to material and process choices. This two-part paper is aimed to understanding how the errors depend on geometric variables related to the shape and orientation of an edge. These variables are usually among the few degrees of freedom allowed at process planning stage, while the choice of material and build parameters is often constrained by either economic reasons or the need to avoid other types of defects.
This objective has received little attention in literature, while issues related to geometric accuracy have been widely studied for surface features (Turner and Gold, 2015). A detailed account of available studies on the topic was given in Part I. Selecting a few references from that review, theoretical insights and experimental results have have been achieved on dimensional errors (e.g. Ziemian and Crawn, 2001; Pérez, 2002; Johnson *et al.*, 2014; Singh, 2014), distortions due to residual stresses (e.g. Zhang and Chou, 2006; Wang *et al.*, 2007; Sood *et al.*, 2009; Peng *et al.*, 2014), geometric deviations due to machine errors (e.g. Agrawal and Dhande, 2007), surface roughness (e.g. Masood *et al.*, 2000; Anitha *et al.*, 2001; Pandey et al., 2003;

Boschetto *et al.*, 2013; Taufik and Jain, 2016), and the control of geometric accuracy by optimization of build orientation (e.g. Thrimurthulu *et al.*, 2004; Ghorpade *et al.*, 2007; Ingole *et al.*, 2011).
Although usually regarded as generic form features, edges may have specific relevance in some applications. For example, errors in the parting lines of prototypes of injection moldings or die castings appear with particular evidence on the silhouette of parts. On some types of parts designed for direct short-run production by AM techniques, inaccurate edges could affect the integrity of small structural sections (e.g. trusses in parts with lattice structures). For machine parts, international standards define the possible deviations from nominal edge geometry (state of an edge) and the related design specifications (ISO, 2000).
Part I has defined a set of geometric variables that describe the local geometry of an edge and can be easily evaluated from the digital model of a part in STL format. A preliminary discussion based on the known constraints of the FDM process has allowed to make conjectures on how the geometric variables influence the position and form errors on the edge. These hypotheses have led a process map where regions corresponding to the likely occurrence of specific error causes are identified within the domain of geometric variables. The process map has been eventually developed into a software procedure, which is able to predict what edges may show visible defects on a part to be built with a given orientation.
Part II reports an experimental investigation with a twofold objective: verify the correctness of the previously formulated prediction criteria, and enhance the scope of the analysis by including estimates of error values for selected combinations of edge-related variables.

2 Definitions and approach

As described in Part I, the local geometric properties of an edge on a part built with a given orientation can be represented by the three following angles (Fig. 1):

- the inclination angle α between the tangent unit vector **t** and the horizontal plane *xy* (perpendicular to the build direction *z*);
- the included angle β between the two adjacent faces in a plane perpendicular to the edge;
- the incidence angle γ between the outward-pointing normal unit vector **n** and the horizontal plane.

These angles are expected to influence the accuracy of the edge along with layer thickness *s* and part height z_0 (for horizontal edges). The possible effects of all the above variables on the geometric errors (i.e. on the deviations from correct edge geometry) have been discussed in Part I, where they have been decomposed in a set of error causes. For each cause, expected influence factors have been identified and theoretical occurrence conditions have been defined. The results of the previous study are summarized in Tab. 1, which includes some terms and equations that will be recalled in the following.
For an experimental verification of the influence of α, β and γ, FDM parts have to be built with many different combinations of the three angles. For this purpose, a part containing an edge with a given value of β can be built in different orientations to obtain different values of α and γ. A build orientation is a transformation from the coordinate frame of the part to the coordinate frame of the build platform. In the initial build orientation (ISO/ASTM, 2013), the *x*, *y* and *z* axes of the two frames coincide. As the deposition process is invariant with respect to rotations about the *z* axis, any part reorientation is defined by a pair of angles φ_x and φ_y, which correspond to two successive rotations about the *x* and *y* axes of the part (Fig. 2a). As proved in Appendix 1, an edge whose tangent and normal are respectively parallel to *x* and *z* in the part coordinate frame (Fig. 2b) yields a given pair (α, γ) under the following build orientation:

$$\varphi_x = \begin{cases} \arccos\dfrac{\sin\gamma}{\cos\alpha} & (\alpha < 90°) \\ 0 & (\alpha = 90°) \end{cases}$$

$$\varphi_y = \alpha$$

Since it has also been shown that

$$|\gamma| \le 90° - \alpha$$

the allowable range of γ gets smaller and smaller with increasing α until it degenerates to a single value ($\gamma = 0$) for $\alpha = 90°$. Uniform ranges can be obtained by the following normalization of the variables:

$$a = \frac{\alpha}{90°} \quad (0 \le a \le 1)$$

$$b = \frac{\beta}{180°} \quad (0 \le b \le 1)$$

$$c = \begin{cases} \dfrac{\gamma}{90° - \alpha}, & \alpha < 90° \\ \text{arbitrary}, & \alpha = 90° \end{cases} \quad (-1 \le c \le 1)$$

On each built part, the edge profile will have to be inspected by measuring the coordinates x_i and z_i ($i = 1, 2, \ldots n$) of n points in the part coordinate frame. Given the nominal dimension z_0 of the edge, the error of the i-th point can be evaluated:

$$e_i = z_i - z_0$$

As shown in Fig. 3, the error can be decomposed into three components considering the average height z_m and the height $z_r(x_i)$ predicted for the point from the least-square regression line of the profile:

$$e_i = [z_m - z_0] + [z_r(x_i) - z_m] + [z_i - z_r(x_i)]$$

Averaging the three terms in square brackets gives three distinct root mean square errors, namely the position error:

$$E_P = z_m - z_0 \tag{1}$$

the orientation error:

$$E_O = \sqrt{\sum_{i=1}^{n} \frac{[z_r(x_i) - z_m]^2}{n}} \tag{2}$$

and the form error:

$$E_F = \sqrt{\sum_{i=1}^{n} \frac{[z_i - z_r(x_i)]^2}{n}} \tag{3}$$

As said before, the above errors on a given edge could depend on the orientation of the part in the FDM process. It must be emphasized, however, that edge accuracy is only one among the possible criteria for the selection of build orientation (a problem that will not be dealt with in this paper). An example of negative correlation with mechanical properties was recently shown on specimens for tensile tests (Torres *et al.*, 2016). In other cases, orientations providing optimum edge accuracy might be unfavourable from a cost perspective due to excessive build time and amount of support material.

3 Experimental plan

The tests for the evaluation of edge quality have been carried out using a Stratasys Fortus 250mc machine. All parts have been built in ABSplus-P430 acrylonitrile butadiene styrene, while the break-away support structures have been built in P400R butadiene-styrene copolymer. Although critical to the detail resolution of the FDM process, the layer thickness has been kept constant to 0.254 mm to focus the attention on the only variables related to edge geometry and orientation.

In order to allow the measurement of edge profiles, each part shall provide an edge and three datum planes defining a coordinate frame for the part. All these features must be in obstacle-free position and have sufficient size. Two different specimens have been designed: the first one, referred to as multiple-angle part (Fig. 4a), has an edge divided into four 7-mm long segments having different included angles ($\beta = 30°$, 60°, 90°, 120°); the second one, referred to as single-angle part (Fig. 4b), is designed in four versions each containing a 22-mm long edge with a different value of the included angle (same values as above). The multiple-angle part allows fast builds and measuring procedures for a preliminary analysis of the effects of edge variables. The single-angle parts allow more accurate measurements due to the longer edge, and they avoid possible inconsistencies of process conditions arising for multiple-angle parts (e.g. support structures may not distribute evenly on the different edge segments). The two specimens have different heights z_0 (20 and 14 mm) to observe possible differences related to nominal dimensions.

The parts have been inspected by a Mitutoyo QV-ELF202 noncontact measuring instrument for 2D profiles. A high-resolution CCD camera acquires an image of the edge placed parallel to the measuring plane. The image is then processed to collect a sequence of points of the profile, whose coordinates are calculated with 0.1-μm resolution and within 2-μm accuracy for the tested part sizes. All the profiles have been sampled with a spacing of 40 μm (25 points per mm), corresponding to 20 pixels of the optical system. A machined fixture has been built to accurately locate three perpendicular datum planes on each part, in order to refer the coordinates of the sample points to the part coordinate frame.

Fig. 5 shows an example of profile reconstruction on a multiple-angle part, whose edge has a 20-mm nominal height on the *xy* reference plane. The procedure automatically divides the profile into individual segments and removes 1-mm long transition zones between consecutive segments. Each resulting segment has 5-mm length and about 125 points, and is individually processed to calculate the errors E_P, E_O and E_F from equations (1-3).

The results of the subplans based on the two specimens are separately reported in the following.

3.1 Tests on the multiple-angle part

The first subplan has been conducted by building the multiple-angle part in a set of different orientations. As shown in Tab. 2, the tests have been planned according to a full factorial design with three factors (the normalized angles *a*, *b*, *c*) with three replications for each of the 32 treatments. The levels of the factors cover the whole domain of inclination angles, including horizontal ($\alpha = 0$) and vertical edges ($\alpha = 90°$). Regarding the included angles, preliminary tests have suggested to avoid either excessively sharp edges ($\beta < 30°$), whose geometry tends to be severely altered due to the finite width of the deposited material (~0.5 mm), and edges with very large angles ($\beta > 120°$), whose quality is not significantly better than in the considered range. The choice of incidence angles has been limited to only upward-pointing edges ($\gamma > 0$) in order to avoid the need for support structures, which would depend on the relative position of the different samples on each built part.

Overall, the subplan has required the production of 24 multiple-angle parts, which were randomly arranged in 4 build runs on the machine. Each run included from 2 to 9 parts, the actual number being set in order to make the build times approximately equal among runs. The choice was justified by the concern that excessive differences in the permanence times of parts at build chamber temperature could bring about disturbances in the geometric errors. Such effects, however, cannot be completely excluded especially for edges with high values of α, and their statistical significance could not be tested due to the low number of treatments.

Fig. 6 shows the effects of the three factors (converted back to unnormalized angles) on the position error. The sample values of E_P are negative for most treatments, i.e. the edge apparently retreats from its nominal position toward the inside of the part. This is not a consequence of material shrinkage but can be explained by the radius effect that will be discussed later. The deviation increases when α increases and β decreases,

while it seems to be less visibly influenced by γ. The analysis of variance on E_P (with $R^2_{adj} = 0.98$) reveals that the individual effects of the three factors are statistically significant along with the double interactions and the triple interaction (actually irrelevant at a visual inspection of response values, not shown in figure). The validity of the analysis is confirmed by the normality of the residuals ($p = 0.26$ in the Anderson-Darling test), the homogeneity of variance ($p = 0.39$ in the Bartlett's test), and the lack of autocorrelation and abnormal trends of the residuals with respect to the three factors and to the fitted response. Appendix 2 gives an overview of the methods used in the analysis of experimental results.

The orientation error E_O has maximum sample values of about 0.03 mm, an order of magnitude below the resolution of the FDM process; it can thus be regarded as negligible for the subplan. For the form error E_F, Fig. 7 shows that only α seems to have a relevant individual effect: sample values are low for horizontal edges, high for slightly inclined edges, and intermediate for more inclined or vertical edges. However, the analysis of variance ($R^2_{adj} = 0.97$) suggests that all the individual and interaction effects are actually significant; again, the analysis of residuals confirms the required normality ($p = 0.25$ in the Anderson-Darling test), homogeneity of variance ($p = 0.92$ in the Levene's test), and lack of autocorrelation and abnormal trends.

3.2 Tests on the single-angle parts

In the second subplan, each version of the single-angle part has been built in a set of different orientations. The full factorial design with 48 treatments is shown in Tab. 3 and includes three replications per treatment. While the levels of α and β are unchanged with respect to the first subplan, the choice of incidence angles now includes laterally-pointing ($\gamma = 0$) and downward-pointing edges ($\gamma < 0$), for which the presence of support structures is predictable as a function of β unlike it is for the multiple-angle part.

The 144 single-angle parts produced in the subplan were randomly arranged in 7 build runs, each including from 8 to 27 parts in the attempt to avoid disturbances related to thermal cycling as previously discussed.

Fig. 8 shows the effects of the unnormalized factors on the position error. As it can be noted by comparison with Fig. 8, positive sample values of E_P are more often observed than for the multiple-angle part, although the average error is still negative. No changes are observed in the effects of α and β, while γ seems to have a more visible effect as E_P takes lower values for laterally-pointing edges. All the individual and interaction effects are confirmed as significant in the analysis of variance ($R^2_{adj} = 0.98$); despite the non-normality of the residuals ($p < 0.01$ in the Anderson-Darling test), the validity of the analysis is supported by both the homogeneity of variance ($p = 0.88$ in the Levene's test) and the lack of autocorrelation and abnormal trends in the residuals.

The orientation error E_O is again negligible, although its sample values are slightly larger than in the first subplan (< 0.05 mm). As shown in Fig. 9, the form error presents the already noted effect of α, and a further visible effect of γ as E_F takes higher values for downward-pointing edges; a less pronounced effect is also observed for β, with higher values of E_F for more acute edges. The analysis of variance on a Box-Cox log transform of the response ($R^2_{adj} = 0.96$) confirms that all of the individual and the interaction effects are significant; although the residuals do not follow a normal distribution ($p < 0.01$ in the Anderson-Darling test), the validity of the analysis is partially supported by the homogeneity of variance ensured by the transformation ($p = 0.31$ in the Levene's test), and by the lack of autocorrelation and abnormal trends of the residuals.

As some factor levels are common to the two subplans, the statistical significance of the differences in the responses has been verified for each of the common treatments (amounting to 16). For the position error, significant differences ($p < 0.05$ in the t-tests) have been obtained for six treatments, half due to small intra-treatment variances and half due to highly different average values; the latter cases include all the treatments with horizontal edges, where the single-angle parts show higher values of E_P. For the form error, eight treatments have shown significant differences due to small intra-treatment variances.

4 Interpretation of results

The above results have been further analyzed in an attempt to validate the error causes discussed in Part I. These causes are related to geometric considerations that may have a role in the calculation of toolpaths by the printing software of the FDM machine; material properties are also shown to influence geometric error values in a few cases. While the previous reasoning relied upon only general knowledge on the FDM process, the same effects can now be recognized by observing the variation of position and form errors with respect to the three angles.

The qualitative trends resulting from experimental tests are shown in Fig. 10 with an indication of the individual error causes that are believed to determine them. It should be noted that form errors have special importance because they can give rise to visually apparent defects on part edges. Position errors are less severe because they do not influence edge appearance unless in very special cases (e.g. curved edges where variable position errors can appear as spurious undulations in an edge profile).

The staircase effect is clearly related to the variation of the form error with α, which suggests the existence of a maximum for small inclination angles. Considerations based on a simplified geometric modeling of the effect (see first row of Tab. 1) suggested that the form error is maximum for nearly horizontal edges ($\alpha = 0+$) and vanishes for horizontal ($\alpha = 0$) and vertical ($\alpha = 90°$) edges. On the built parts, the maximum form error is actually observed for small inclination angles, but the small number of experimental levels does not allow to locate it exactly. Error values are always greater than zero and, as expected, are slightly higher for vertical than for horizontal edges due to the curvature of the free boundary of the deposited strand.

A magnified image of a built part with $\alpha = 90°$ (Fig. 11a) shows the typical appearance of the form error occurring due to the staircase effect: the profile shows periodic waves having length and amplitude in the order of the layer thickness. On a part with $\alpha = 30°$ (Fig. 11b), the amplitude of the waves is larger and an additional waviness with two-layer length is also evident. At a naked-eye observation, the effect is almost invisible on the former edge, while the latter edge appears jagged but fairly regular in shape.

The support effect is most probably related to the variation of the form error as a function of γ, because edges pointing downwards ($\gamma < 0$) are more likely to require supports that can leave marks on the part after they are removed. Although less obviously, the same effect might also explain the variation of the position error as a function of γ, which has a maximum negative value for laterally pointing edges. In this condition, a thinner web is likely to develop next to the edge, and small fragments of materials are more easily pulled out of the edge during support removal; as a consequence, parts of the edge move backwards from their nominal position.

The magnified image of a built part with $\gamma = -60°$ (Fig. 12) shows that the form error due to the support effect (here superimposed to the staircase effect) typically consists in isolated dents with variable length and depth in the order of layer thickness. At a naked-eye observation, the edge may appear seriously irregular in shape.

The radius effect explains the variation of the position error with β, which is consistent with previous considerations based on geometric reasoning (third row of Tab. 1): lower included angles cause higher negative values of the position errors because the apex of the toolpath gets farther from the nominal position of the edge. A similar occurrence for low values of α, which was expected due to the decrease of the effective bend angle, is a negligible effect compared to other error causes with opposite influence (offset and swelling effects).

The combined effect of the offset trajectories and the curved free boundaries explains why the negative position error actually increases with α. As it was suggested by geometric considerations, at low values of α the layer boundaries can partially overlap the nominal profile and reduce the negative value of the position error, possibily leading to an inverted (i.e. positive) position error.

The inversion of the position error for low values of α can have a further explanation, which is also consistent with the significant differences in the position error observed on the two specimens. As almost all

differences involve horizontal edges ($\alpha = 0$), it can be conjectured that the average height of the profile is more likely to be in excess of the nominal height z_0 when the edge lies on a single layer. This appears to be caused by swelling, i.e. the expansion of the material along z due to the recovery of elastic strains accumulated when the thermoplastic resin is extruded through the nozzle. The difference between the specimens suggests that the slicing error also plays a role for horizontal edges; it actually takes different values due to the different nominal dimensions (fifth row of Tab. 1):

$$d_1 = s \cdot \lfloor z_0/s \rfloor - z_0 = \begin{cases} 0.254 \cdot 78 - 20 = -0.19 \text{ mm} & \text{(multiple-angle part)} \\ 0.254 \cdot 55 - 14 = -0.03 \text{ mm} & \text{(single-angle parts)} \end{cases}$$

The above discussion has attempted to explain the only influence of geometric variables related to edges. It cannot be excluded, however, that the same error causes can depend on the choice of process parameters, which has not been considered in this paper. Tab. 4 lists some tentative hypotheses about the influence of some parameters, suggesting whether the severity of the different error causes are expected to increase (+) or decrease (–) with the value of each parameter. Specifically:

- thinner layers obviously reduce staircasing, offset and slicing error, but should also have indirect positive effects on the radius effect (due to the decrease of bend radius) and on swelling (because each single layer swells separately);
- slower speeds involve less swelling (as observed in conventional extrusion), but may also reduce the need of supports (due to a lower average temperature of the material behind the extrusion nozzle);
- higher temperatures should reduce stress and distortion on the free boundaries of layers, thus alleviating several error causes (staircase, offset, swelling).

Future investigations will have to confirm the significance of the expected effects.

5 Conclusions

The experimental verification confirms the findings reported in Part I. The key conclusion is that position and form errors have systematic components that depend on the three angles defining the geometry and orientation of an edge. Specifically:

- edges with inclination angle below 30° and any included angle are severely affected by the staircase effect, which causes a regularly jagged appearance;
- edges with low incidence angles (either negative or below a threshold increasing with decreasing included angles) can show support marks with possibly irregular appearance;
- the position of an edge can be notably displaced toward the inside of the part if either the included angle is lower than about 60° (radius effect), the inclination angle is greater than about 60° (offset and curved-boundary effect), or the incidence angle is nearly zero (support effect); on the contrary, edges with zero inclination angle are usually displaced toward the outside;
- for a 0.254-mm layer thickness, the form error can be visible at values below 0.1 mm, while the position error can reach 0.3-0.4 mm with no special impact on edge appearance.

Future developments of the work will have to overcome the limitations of the reported experimental tests. These include the use of only one setting (FDM machine, materials and layer thickness), which can be regarded as typical for prototyping work; it would be interesting to verify whether similar results apply to different settings common in high-end industrial applications or in consumer-grade 3D printing. Further investigations could also be conducted to better understand the role of process parameters such as layer thickness, deposition speed and melt temperature. With a stronger focus on applications, the definition of edge quality will possibly be extended including the need to ensure a uniform appearance (and not only low average deviations) along edges with special aesthetic requirements.

Appendix 1: Calculation of orientation parameters

The build orientation that allows to get given angles α and γ on an edge is to be calculated. As an orientation is identified by two consecutive rotations about the x and y axes, the problem consists in calculating the two rotation angles φ_x and φ_y. With reference to Fig. 2b, let an edge have the following tangent and normal unit vectors:

$$\mathbf{t} = \begin{bmatrix} 1 \\ 0 \\ 0 \end{bmatrix}, \quad \mathbf{n} = \begin{bmatrix} 0 \\ 0 \\ 1 \end{bmatrix}$$

As an effect of the two rotations, the two vectors transform into

$$\mathbf{t}' = R_y \cdot R_x \cdot \mathbf{t}$$
$$\mathbf{n}' = R_y \cdot R_x \cdot \mathbf{n}$$

where

$$R_y \cdot R_x = \begin{bmatrix} \cos\varphi_y & 0 & \sin\varphi_y \\ 0 & 1 & 0 \\ -\sin\varphi_y & 0 & \cos\varphi_y \end{bmatrix} \cdot \begin{bmatrix} 1 & 0 & 0 \\ 0 & \cos\varphi_x & -\sin\varphi_x \\ 0 & \sin\varphi_x & \cos\varphi_x \end{bmatrix} = \begin{bmatrix} \cos\varphi_y & \sin\varphi_x \sin\varphi_y & \cos\varphi_x \sin\varphi_y \\ 0 & \cos\varphi_x & -\sin\varphi_x \\ -\sin\varphi_y & \sin\varphi_x \cos\varphi_y & \cos\varphi_x \cos\varphi_y \end{bmatrix}$$

This gives

$$\mathbf{t}' = \begin{bmatrix} \cos\varphi_y \\ 0 \\ -\sin\varphi_y \end{bmatrix}, \quad \mathbf{n}' = \begin{bmatrix} \cos\varphi_x \sin\varphi_y \\ -\sin\varphi_x \\ \cos\varphi_x \cos\varphi_y \end{bmatrix}$$

By definition of the angles α and γ it results that

$$\sin\alpha = |t'_z| = |-\sin\varphi_y| \rightarrow \quad \varphi_y = \alpha$$

$$\sin\gamma = n'_z = \cos\varphi_x \cos\varphi_y = \cos\varphi_x \cos\alpha \rightarrow \quad \varphi_x = \arccos\left(\frac{\sin\gamma}{\cos\alpha}\right)$$

Appendix 2: Statistical analysis of experimental data

The experimental tests reported in the paper have been planned and interpreted according to the methodology of Design and Analysis of Experiments (DOE). Each of the two subplans described in Section 3 is a full factorial plan with 3 factors (a, b, c); this means that each factor can take a given number of values (levels), and the values of each response (the measured errors E_P, E_O, E_F) are collected for every combination of factor levels (treatments). As each treatment is tested a given number of times (replications), different values of the responses are usually obtained both among different treatments and within the same treatment. The analysis of the factorial plan aims to verifying whether the differences in response values among treatments are statistically significant, i.e. cannot be neglected compared to differences within treatments.

The method used for this purpose is the Analysis of Variance (ANOVA), which is based on the comparison among sample statistics on the values of the response. Each statistic is a mean square error, i.e. a sum of squared errors (differences of response values from reference averages) divided by an appropriate number of degrees of freedom. By properly choosing the averages, a three-factor ANOVA calculates the mean square errors related to:

- the individual effects of the factors (a, b, c);

- the interaction effects between pairs of factors (*a*-*b*, *a*-*c*, *b*-*c*);
- the triple interaction effect among the factors (*a*-*b*-*c*);
- the errors within the same treatment.

The effects are tested for significance by comparing their mean squares with the error mean square by variance-comparison tests (F-tests, p-value < 0.05). The adjusted coefficient of determination R^2_{adj} is defined so as to take values close to 1 when the intra-treatment errors are negligible.

The correctness of ANOVA results must be proved by the analysis of residuals (differences between response values and estimated values excluding the statistical errors). The following conditions on the residuals are verified by suitable statistical tests:

- normality (Anderson-Darling test);
- homogeneity of variance, i.e. independence of the residuals on factor levels (Bartlett's or Levene's test);
- lack of autocorrelation, i.e. no visible pattern in the time sequence of measured values;
- lack of abnormal trends when plotting residuals against factor levels.

The failure of the tests on the residuals (p-value < 0.05) can require the replacement of the response with a mathematical function of it (e.g. power or logarithm), as suggested by a suitable procedure (Box-Cox transformation).

See appropriate textbooks (e.g. Montgomery, 2012) for further details on the above cited methods.

Acknowledgements

The authors are grateful to Pasquale Aquilino (Politecnico di Milano) and Timothy Minton (Brunel University) for their help and advice.

References

Agrawal S. and Dhande S.G. (2007), "Analysis of mechanical error in a fused deposition process using a stochastic approach", *International Journal of Production Research*, Vol. 45 No. 17, pp. 3991-4012.

Anitha R., Arunachalam S. and Radhakrishnan P. (2001), "Critical parameters influencing the quality of prototypes in fused deposition modelling", *Journal of Materials Processing Technology*, Vol. 118, pp. 385-388.

Boschetto A., Giordano V. and Veniali F. (2013), "3D roughness profile model in fused deposition modelling", *Rapid Prototyping Journal*, Vol. 19 No. 4, pp. 240-252.

Ghorpade A., Karunakaran K.P. and Tiwan M.K. (2007), "Selection of optimal part orientation in fused deposition modelling using swarm intelligence", *Proceedings IMechE Part B: Journal of Engineering Manufacture*, Vol. 221, pp. 1209-1220.

Ingole D.S., Deshmukh T.R., Kuthe A.M. and Ashtankar K.M. (2011), "Build orientation analysis for minimum cost determination in FDM", *Proceedings IMechE Part B: Journal of Engineering Manufacture*, Vol. 225, pp. 1925-1938.

ISO 13715 (2000), "Technical drawings: edges of undefined shape, vocabulary and indications", International Organization for Standardization, Geneva, Switzerland.

ISO/ASTM 52921 (2013), Standard terminology for additive manufacturing. Coordinate systems and test methodology, ASTM International, West Conshohocken, PA.

Johnson W.J., Rowell M., Deason B. and Eubanks M. (2014), "Comparative evaluation of an open-source FDM system", *Rapid Prototyping Journal*, Vol. 20 No. 3, pp. 205-214.

Masood S.H., Rattanawong W. and Iovenitti P. (2000), "Part build orientations based on volumetric error in fused deposition modelling", *International Journal of Advanced Manufacturing Technology*, Vol. 16, pp. 162-168.

Montgomery D.C. (2012), *Design and analysis of experiments*, Wiley, New York.

Pandey P.M., Venkata Reddy N., Dhande S.G. (2003), "Improvement of surface finish by staircase machining in fused deposition modeling", *Journal of Materials Processing Technology*, Vol. 132, pp. 323-331.

Peng A., Xiao X. and Yue R. (2014), "Process parameter optimization for fused deposition modeling using response surface methodology combined with fuzzy inference system", *International Journal of Advanced Manufacturing Technology*, Vol. 73, pp. 87-100.

Pérez C.J.L. (2002), "Analysis of the surface roughness and dimensional accuracy capability of fused deposition modelling processes", *International Journal of Production Research*, Vol. 40 No. 12, pp. 2865-2881.

Singh R. (2014), "Process capability analysis of fused deposition modelling for plastic components", *Rapid Prototyping Journal*, Vol. 20 No. 1, pp. 69-76.

Sood A.K., Ohdar R.K. and Mahapatra S.S. (2009), "Parametric appraisal of fused deposition modelling process using the grey Taguchi method", *Proceedings IMechE Part B: Journal of Engineering Manufacture*, Vol. 224, pp. 135-145.

Taufik M., Jain P.K. (2016), "A study of build edge profile for prediction of surface roughness in fused deposition modeling", *ASME Journal of Manufacturing Science and Engineering*, Vol. 138, 061002.

Thrimurthulu K., Pandey P.M. and Reddy N.V. (2004), "Optimum part deposition orientation in fused deposition modeling", *International Journal of Machine Tools and Manufacture*, Vol. 44, pp. 585-594.

Torres J., Cole M., Owji A., DeMastry Z., Gordon A.P., "An approach for mechanical property optimization of fused deposition modeling with polylactic acid via design of experiments", *Rapid Prototyping Journal*, Vol. 22 No. 2, pp. 387-404.

Turner B.N. and Gold S.A. (2015), "A review of melt extrusion additive manufacturing processes: II. Materials, dimensional accuracy and surface roughness", *Rapid Prototyping Journal*, Vol. 21 No. 3, pp. 250-261.

Wang T.M., Xi J.T. and Jin Y. (2007), "A model research for prototype warp deformation in the FDM process", *International Journal of Advanced Manufacturing Technology*, Vol. 33, pp. 1087-1096.

Zhang Y. and Chou Y.K. (2006), "Three-dimensional finite element analysis simulations of the fused deposition modelling process", *Proceedings IMechE Part B: Journal of Engineering Manufacture*, Vol. 220, pp. 1663-1671.

Ziemian C.W. and Crawn P.M. III (2001), "Computer aided decision support for fused deposition modeling", *Rapid Prototyping Journal*, Vol. 7 No. 3, pp. 138-147.

List of figures

List of tables

Part II – Tab. 1

Effect	*Description*	*Expected factors*	*Theoretical estimate or condition*
Staircase	Edge profile has a jagged appearance due to the stacking of layers	s, α	Depth of grooves: $h = \begin{cases} s \cdot \cos\alpha\,, & \alpha > 0 \\ 0\,, & \alpha = 0 \end{cases}$
Support	Removal of support material leaves marks on edge profile	β, γ	Supports are required if: $\delta = 90° - \gamma - \beta/2 > 40 - 60°$
Radius	Rounded bend in deposition trajectory makes edge retract from nominal position	s, β	Deviation from nominal position: $d = s \cdot \left(\frac{1}{\sin \beta/2} - 1 \right),\ \ 0 < \beta < 180°$
Offset, curved boundary	Deposition trajectory is offset from nominal edge position due to curved free boundary	α	Position error decreasing when α increases
Slicing	Height of horizontal edges is limited to multiples of layer thickness	s, z_0	Deviation from nominal height: $d_1 = s \cdot \lfloor z_0/s \rfloor - z_0 \le 0$
Swelling	Height of horizontal edges increases due to material viscoelasticity	–	Deviation from nominal height: $d_2 > 0$

Part II – Tab. 2

Factor	*Symbol*	*Levels*
Normalized inclination angle	a	0, 1/3, 2/3, 1
Normalized included angle	b	1/6, 1/3, 1/2, 2/3
Normalized incidence angle	c	1/2, 1

Part II – Tab. 3

Factor	*Symbol*	*Levels*
Normalized inclination angle	a	0, 1/3, 2/3, 1
Normalized included angle	b	1/6, 1/3, 1/2, 2/3
Normalized incidence angle	c	–1, 0, 1

Part II – Tab. 4

Process parameter	*Expected influence on errors due to:*					
	staircase	*support*	*radius*	*offset*	*slicing*	*swelling*
Layer thickness	+		+	+	+	+
Deposition speed		+				+
Melt temperature	–			–		–

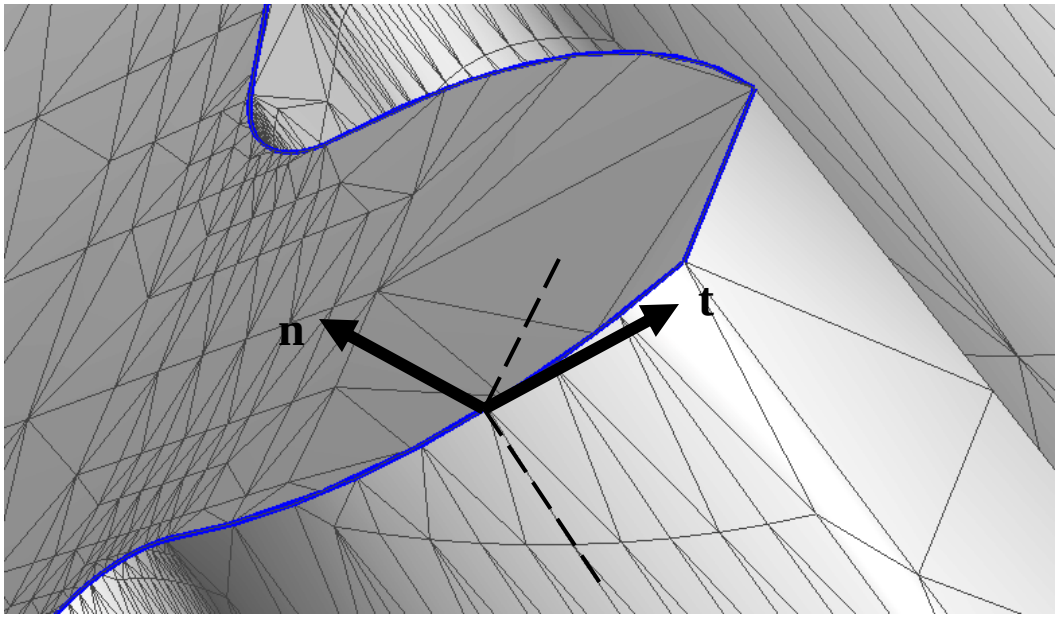

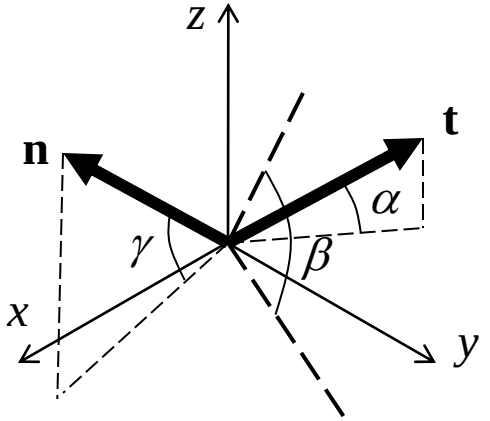

Part II – Fig. 1

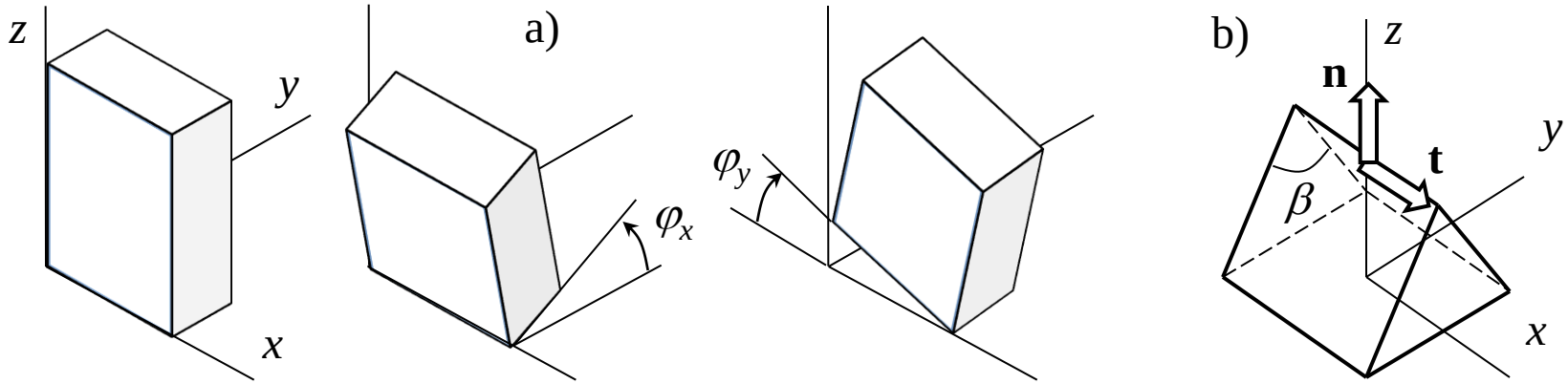

Part II – Fig. 2

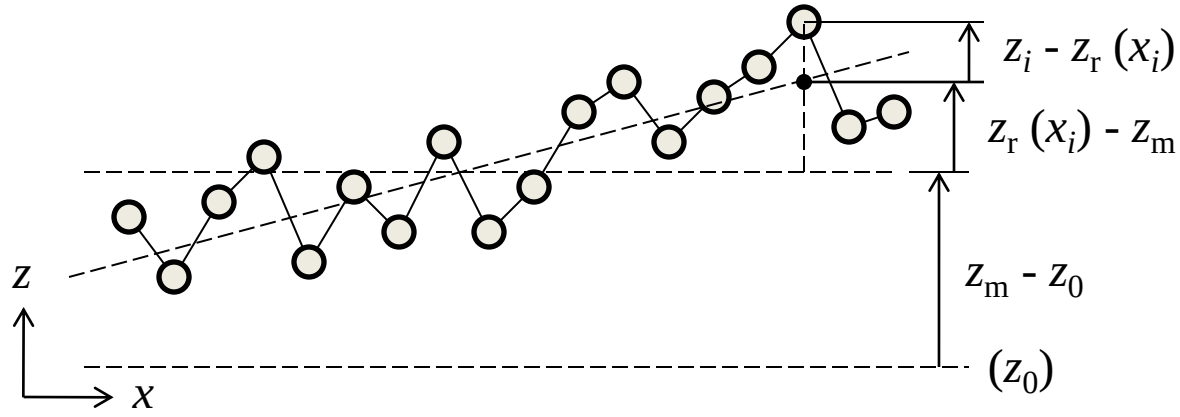

Part II – Fig. 3

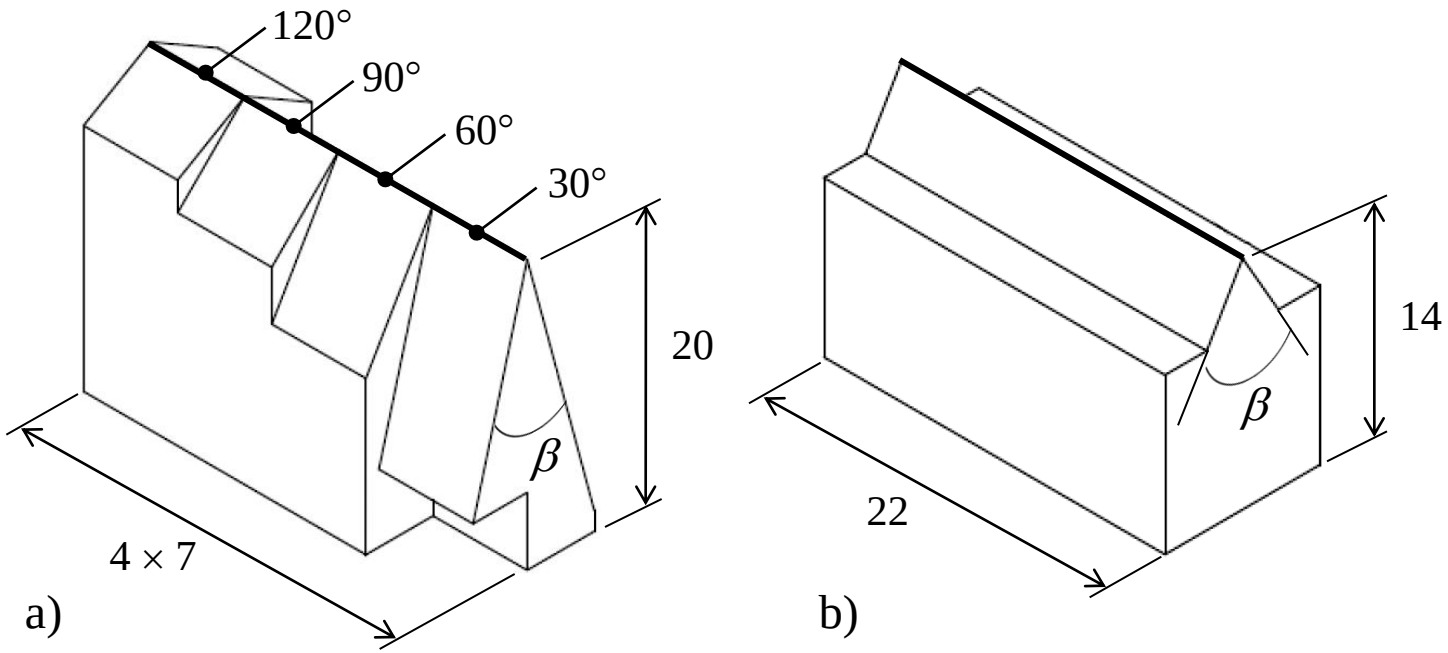

Part II – Fig. 4

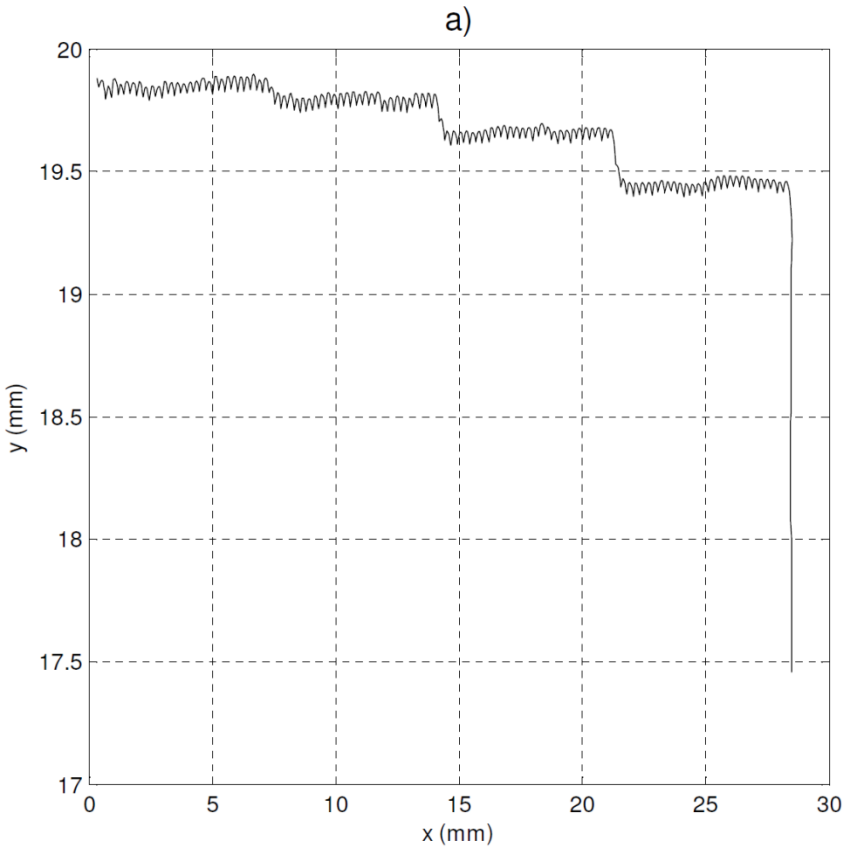
a)
20
19.5
19
18.5
18
17.5
17
y (mm)
0
5
10
15
20
25
30
x (mm)

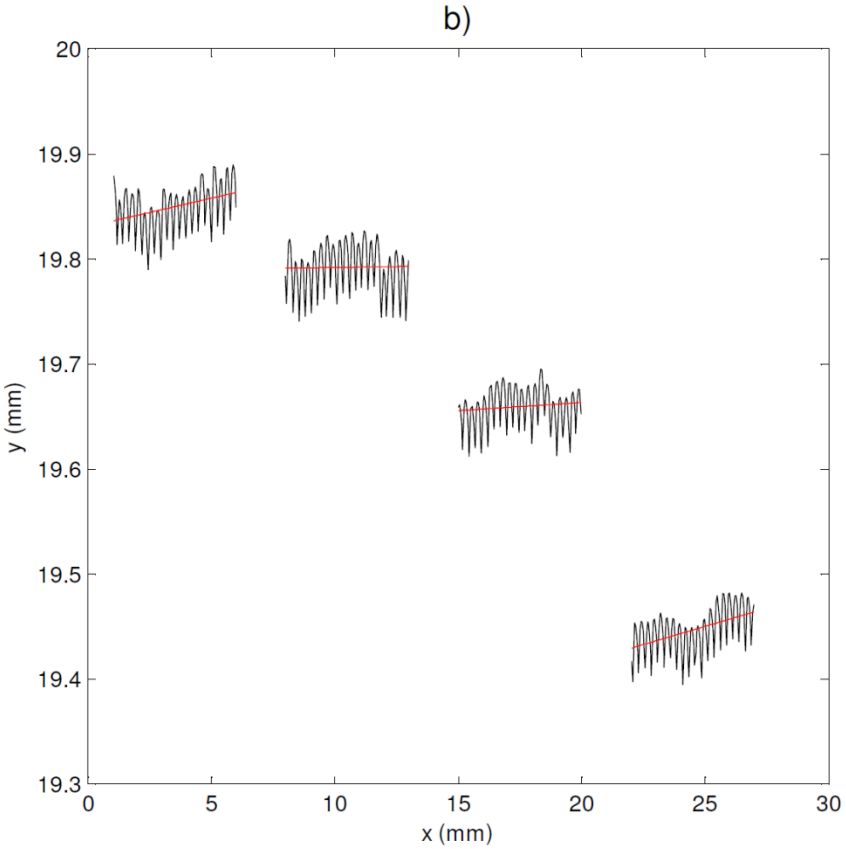
b)
20
19.9
19.8
19.7
19.6
19.5
19.4
19.3
y (mm)
0
5
10
15
20
25
30
x (mm)

Part II – Fig. 5

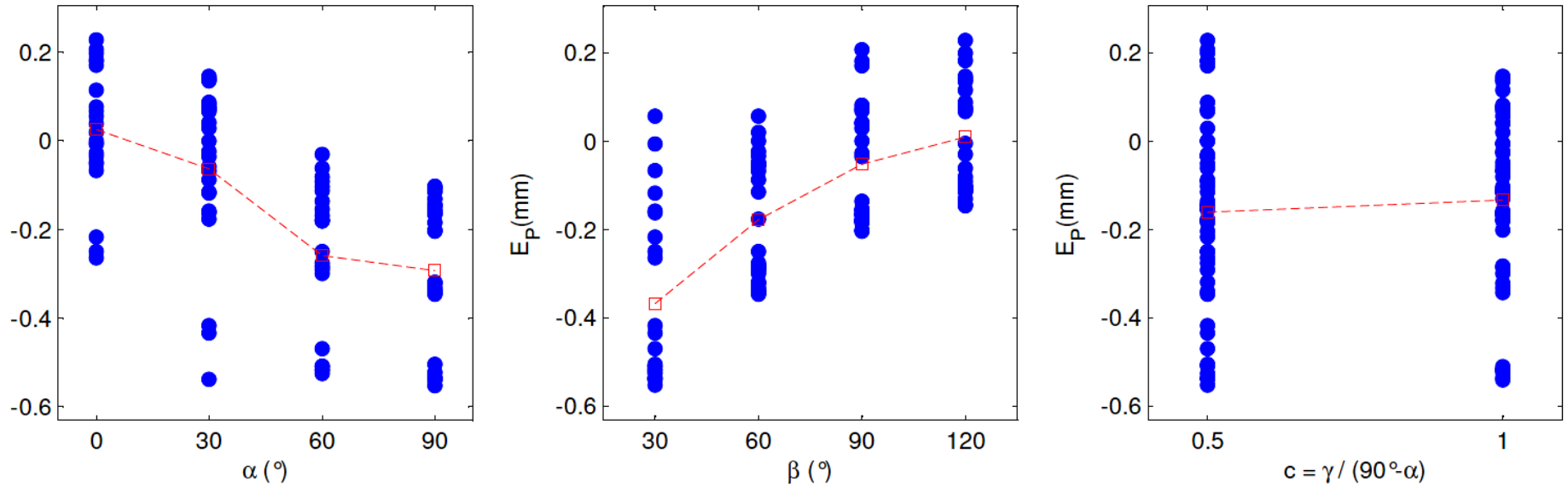

Part II – Fig. 6

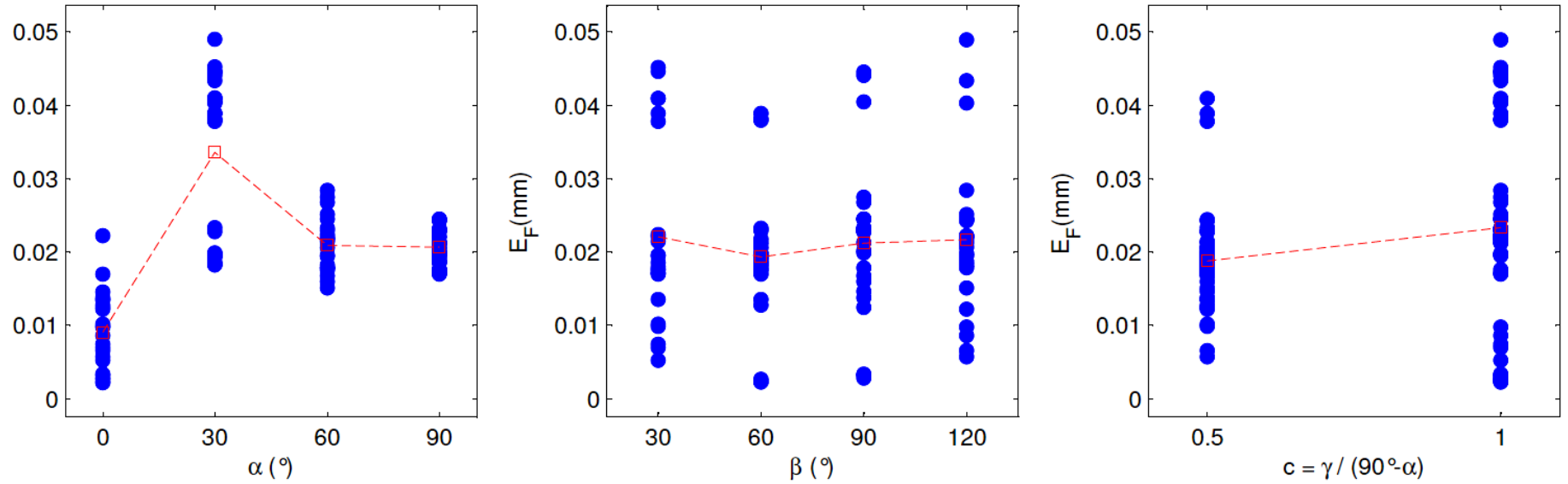

Part II – Fig. 7

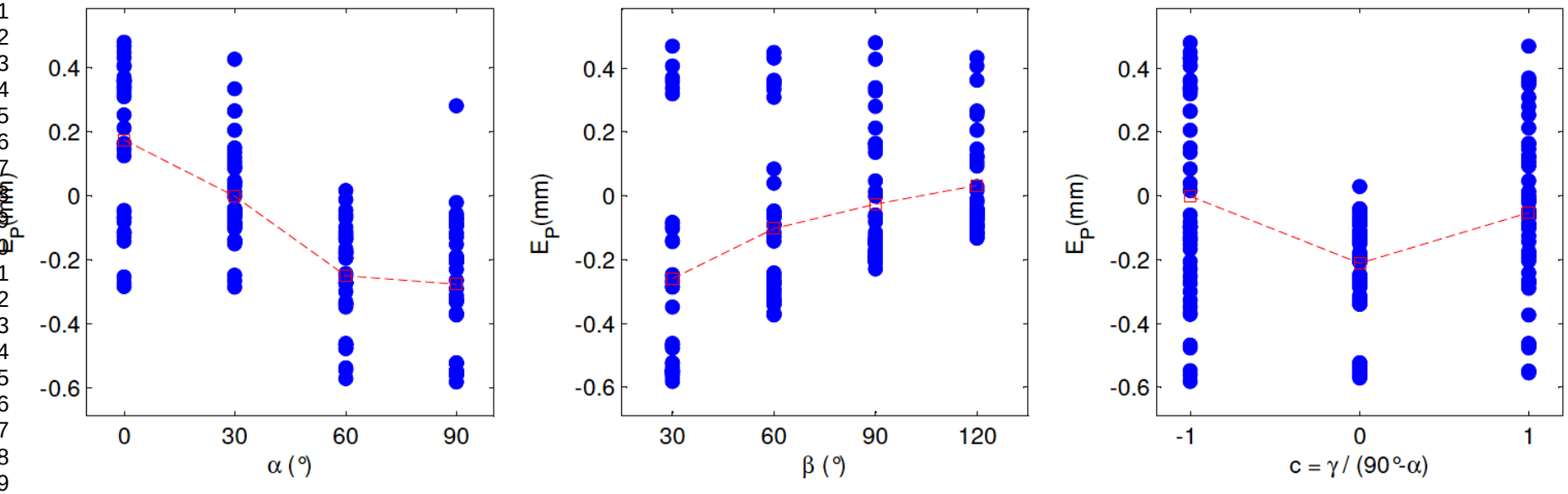

Part II – Fig. 8

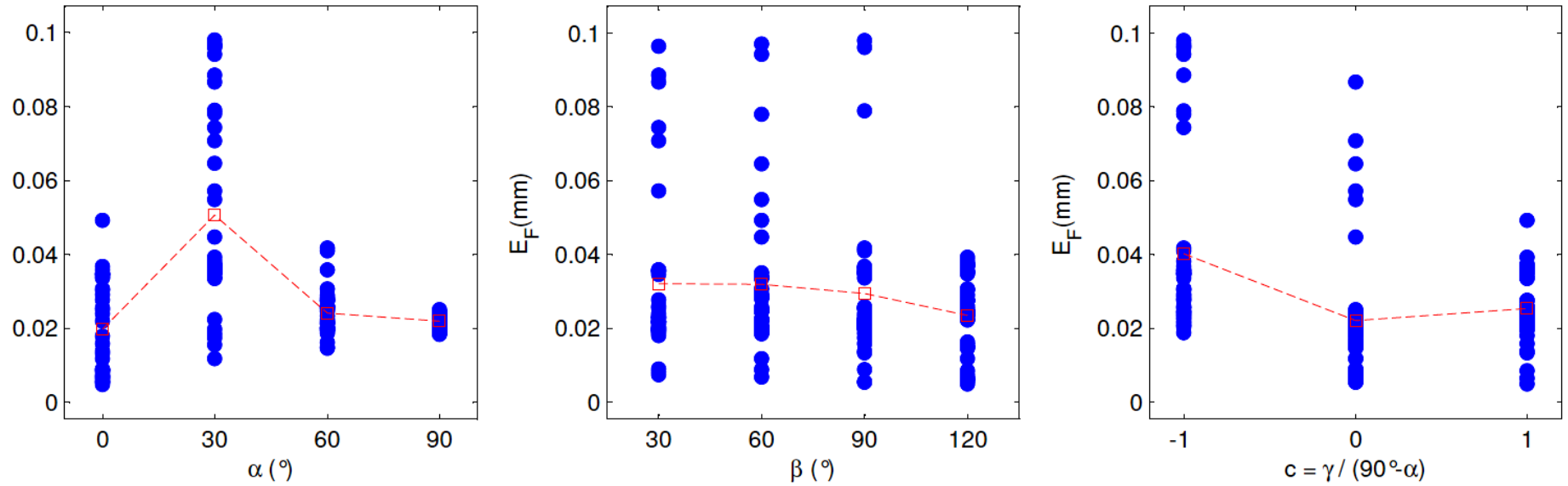

Part II – Fig. 9

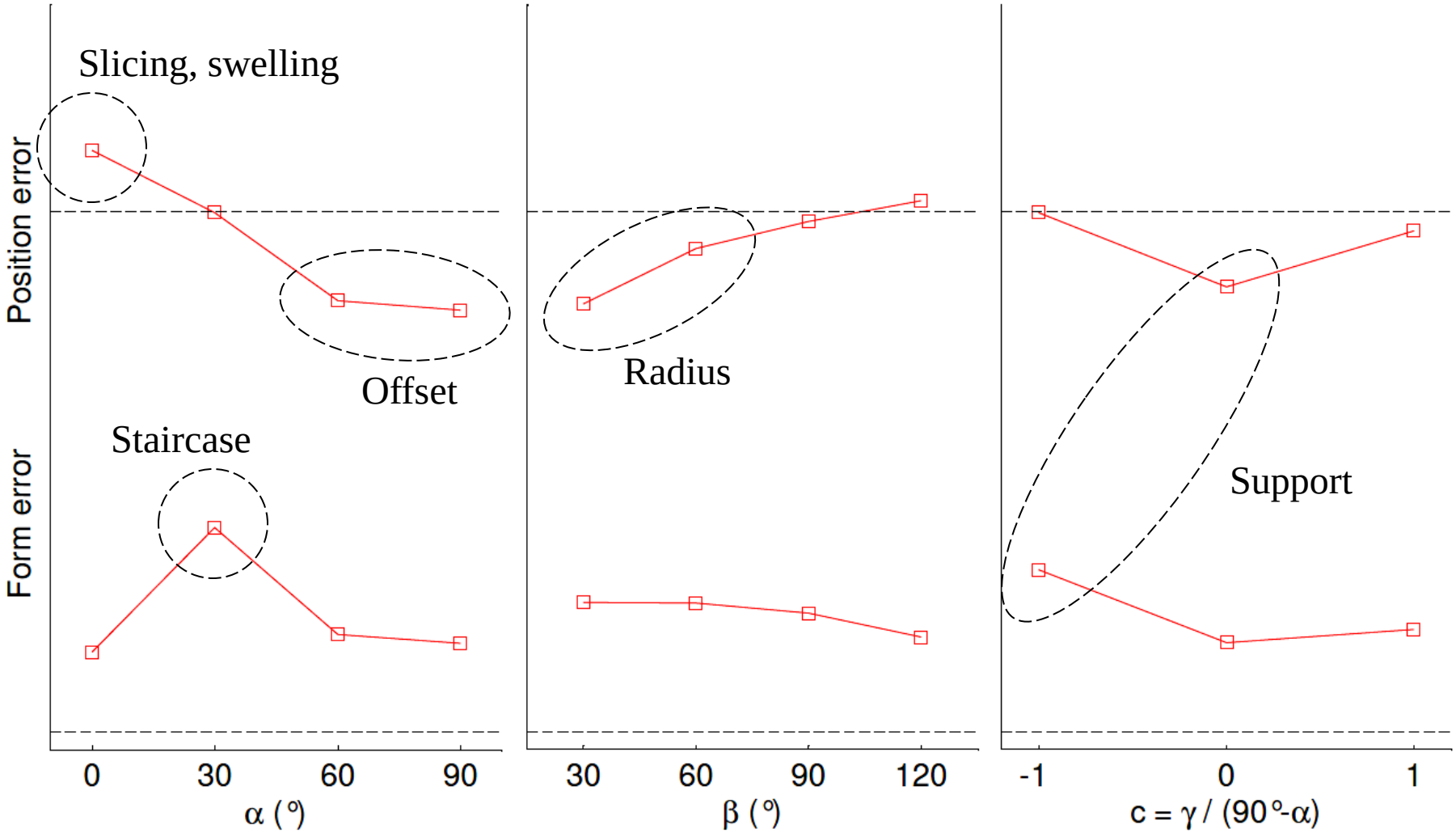

Part II – Fig. 10

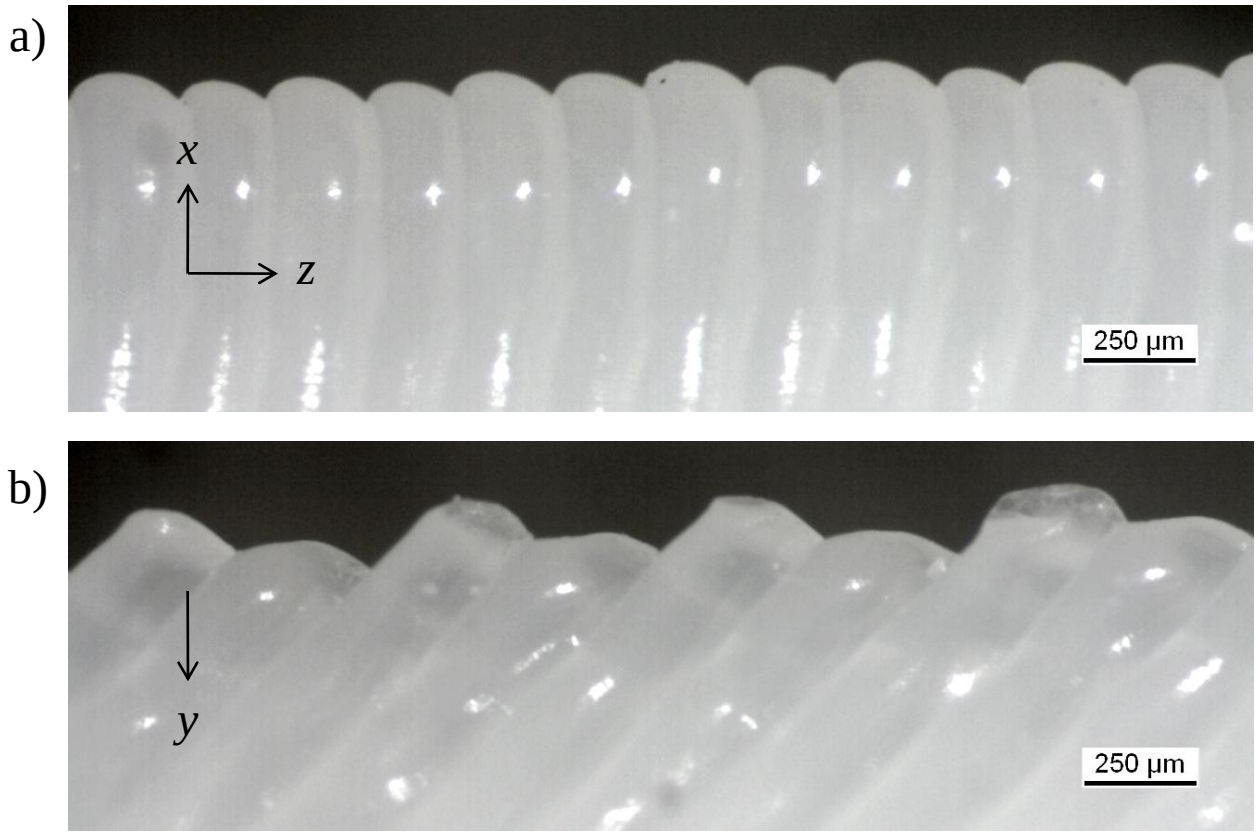

Part II – Fig. 11

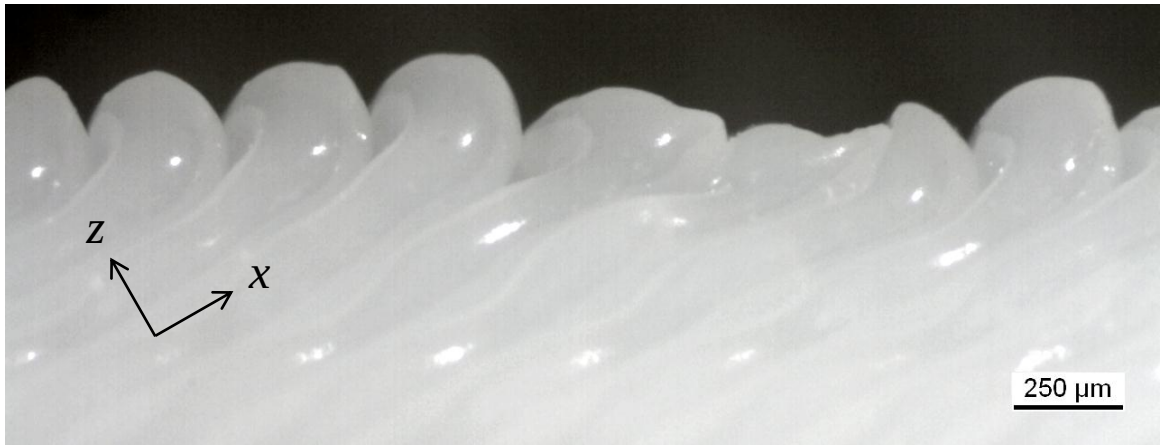

Part II – Fig. 12